PHYSICAL REVIEW B **88**, 144510 (2013)

BCS-like superconductivity in the noncentrosymmetric compounds Nb_xRe_{1-x} ($0.13 \leqslant x \leqslant 0.38$)

J. Chen,[1] L. Jiao,[1] J. L. Zhang,[1] Y. Chen,[1] L. Yang,[1] M. Nicklas,[2] F. Steglich,[2] and H. Q. Yuan[1,*]

[1]*Center for Correlated Matter and Department of Physics, Zhejiang University, Hangzhou, Zhejiang 310027, China*

[2]*Max Planck Institute for Chemical Physics of Solids, D-01187 Dresden, Germany*

(Received 21 August 2013; revised manuscript received 1 October 2013; published 21 October 2013)

We present research on the superconducting properties of Nb_xRe_{1-x} ($x = 0.13$–0.38) obtained by measuring the electrical resistivity $\rho(T)$, magnetic susceptibility $\chi(T)$, specific heat $C_P(T)$, and London penetration depth $\Delta\lambda(T)$. It is found that the superconducting transition temperature T_c decreases monotonically with an increase of x. The upper critical field $B_{c2}(T)$ for various x can be nicely scaled by its corresponding T_c. The electronic specific heat $C_e(T)/T$, penetration depth $\Delta\lambda(T)$, and superfluid density $\rho_s(T)$ demonstrate exponential behavior at low temperatures and can be well fitted by a one-gap BCS model. The residual Sommerfeld coefficient $\gamma_0(B)$ in the superconducting state follows a linear field dependence. All these properties suggest an s-wave BCS-type of superconductivity with a very large $B_{c2}(0)$ for Nb_xRe_{1-x} ($0.13 \leqslant x \leqslant 0.38$).

DOI: 10.1103/PhysRevB.88.144510 PACS number(s): 74.70.Ad, 74.25.Bt, 74.25.N−

I. INTRODUCTION

The discovery of superconductivity (SC) in the heavy fermion compound $CePt_3Si$ has attracted considerable interest in studying the effects of broken inversion symmetry on superconducting pairing states.[1] While the inversion symmetry is absent in a crystal, the resulting antisymmetric potential gradient causes a parity-breaking antisymmetric spin-orbit coupling (ASOC), which may lift up the spin degeneracy. An admixture of spin-singlet and spin-triplet components is then allowed in the pairing states, whose ratio might be tuned by the ASOC strength.[2–6] Such a scenario seems to be supported by the experimental observations of $Li_2(Pd_{1-x}Pt_x)_3B$, in which evidence of BCS-like SC is shown in Li_2Pd_3B, but a spin triplet was recognized in Li_2Pt_3B with increasing ASOC strength.[7–9] Furthermore, noncentrosymmetric (NCS) superconductors were recently proposed as important candidates for studying topological SC.[10,11]

In the past few years, a growing number of NCS superconductors have been studied, varying from heavy fermion compounds to a number of weakly correlated intermetallic compounds.[12] Exotic properties, including nodal SC,[7,13–15] multigap SC,[16–19] and a huge upper critical field,[15,20,21] have been experimentally observed in these systems. However, the role of lacking inversion symmetry on the superconducting pairing states remains a fundamentally open question.[19] Therefore, it is highly desirable to elucidate the determining parameters of the pairing state in NCS superconductors. Systematic studies on the superconducting properties of NCS superconductors with a tunable ASOC strength may help address these issues.

The intermetallic binary compound Nb_xRe_{1-x} ($0.13 \leqslant x \leqslant 0.38$) crystallizes in the cubic Ti_5Re_{24}-type structure with a space group $I\bar{4}3m$ (No. 217), which loses inversion symmetry on the sites of Nb($24g$) and Re($24g$). SC was initially reported in these compounds by Knapton *et al.* in the 1950's.[22] Very recently, the superconducting properties of $Nb_{0.18}Re_{0.82}$ were revisited as an example of NCS superconductors; both specific-heat and NMR experiments indicated an s-wave type SC.[23,24] In order to provide further characterizations of the superconducting pairing state and its evolution as a function of x in Nb_xRe_{1-x}, we synthesized a series of polycrystals with varying Nb content, which are expected to modify the ASOC strength due to the very different atomic numbers of Nb and Re. The superconducting properties are systematically studied by measuring the electrical resistivity $\rho(T)$, magnetic susceptibility $\chi(T)$, specific heat $C_p(T,B)$, as well as the London penetration depth $\Delta\lambda(T)$. Our results provide strong evidence of BCS-like SC for Nb_xRe_{1-x}.

II. EXPERIMENTAL METHODS

Polycrystalline Nb_xRe_{1-x} ($x = 0.13$–0.93) samples were prepared by a two-step arc melting method in ultrapure argon gas. A Ti button was used as an oxygen getter. In the first step, buttons of high-purity niobium (99.99%, Alfa Aesar) and rhenium (99.99%, Alfa Aesar) powders were prepared by arc melting, respectively. In the second step, stoichiometric amounts of the two compositions were melted together to form the alloy Nb_xRe_{1-x}. The ingot was inverted and remelted several times to improve sample homogeneity. Such a two-step approach is efficient to decrease the melting points of materials through alloying. The so-derived ingot forms a hard button with a negligible weight loss of less than 0.5%, attributed to the low vapor pressure of Nb and Re. A subsequent heat treatment was performed at 800 °C in a vacuum-sealed quartz tube for 7 days, followed by a slow cooling of the furnace.

The crystal structure of the ingots was characterized by powder x-ray diffractometry (XRD) using a X'Pert PRO diffractometer (Cu$K\alpha$ radiation) in the Bragg-Brentano geometry for the 2Θ range of 10°–90°. Sample compositions were identified by using energy dispersive x-ray (EDX) spectroscopy, showing nearly the same compositions as the nominal values. The electrical resistivity was measured using a standard four-probe method in a dc magnetic field up to 14 T and at temperatures down to 0.3 K in a ^{3}He cryostat. Measurements of the magnetic susceptibility and specific heat were performed in a commercial magnetic property measurement system (5T-MPMS) and a physical property measurement system (9T-PPMS) (Quantum Design), respectively. Measurements of the London penetration depth $\Delta\lambda(T)$ were performed by using a technique based on a tunnel

diode oscillator (TDO)[25] at a frequency of 7 MHz down to 0.4 K in a ^{3}He cryostat.

III. RESULTS AND DISCUSSION

A. Crystal structures

Powder XRD spectra were taken on the Nb_xRe_{1-x} samples with various x ($x = 0.13$–0.93) at room temperature. It was found that Nb_xRe_{1-x} crystallizes in three different crystal structures while varying the Nb composition from $x = 0.13$ to $x = 0.93$, which is consistent with previous reports.[22] For $0.13 \leqslant x \leqslant 0.38$ (region I), XRD patterns identify our samples as being of single phase with a cubic Ti_5Re_{24} structure [see Fig. 1(a)]. In each unit cell, there are 58 atoms on four crystallographically distinct sites: Nb(1), Nb(2), Re(1), and Re(2) [see the inset of Fig. 1(b)]. The inversion symmetry is preserved for the Nb(1) sites ($2a$), occupied by two Nb atoms, while it is broken on the Nb(2), Re(1), and Re(2) sites along all crystallographic directions, which are occupied by 8 Nb, 24 Re, and 24 Re atoms, respectively. For $0.38 < x \leqslant 0.52$ (region II), the Nb_7Re_8-type phase dominates (tetragonal, $P4_2/mnm$). However, XRD patterns reveal a Nb structure with cubic $Im\bar{3}m$ space group (No. 229) in the range of $0.55 \leqslant x \leqslant 0.93$, demonstrating a maximum solubility of 46% rhenium in niobium.[22] In regions I and II, there is a systematic shift of the diffraction peaks to lower angles with increasing x, suggesting a binary solid solution for Nb_xRe_{1-x} ($x = 0.13$–0.54). It is noted that the Nb_xRe_{1-x} alloys are mixed with Nb_5Re_{24} and Re-element phases for $0 < x < 0.13$.[22] In this paper, we will mainly focus on the properties of the NCS superconductors in region I.

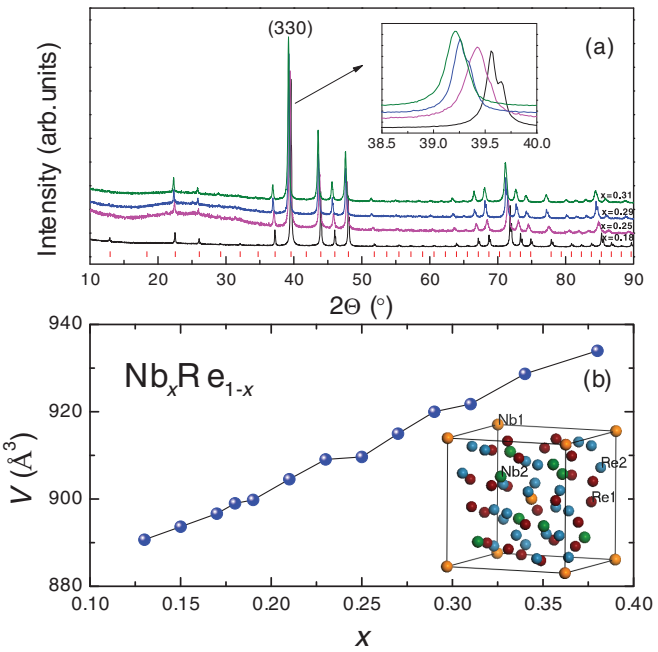

FIG. 1. (Color online) (a) XRD patterns for Nb_xRe_{1-x}, $x = 0.18$, 0.25, 0.29, and 0.38. Short vertical bars are the standard reflection positions. (b) The unit cell volume plotted as a function of x for samples with $x = 0.13$–0.38. The inset shows the Ti_5Re_{24}-type crystal structure.

In Fig. 1(b), we plot the unit cell volume V as a function of x for Nb_xRe_{1-x} ($0.13 \leqslant x \leqslant 0.38$), as determined from the XRD patterns using Rietveld refinement. One can see that the unit cell volume increases monotonically with increasing x, attributed to the larger atomic radius of Nb. We find a lattice parameter of $a = 9.6507$ Å for $Nb_{0.18}Re_{0.82}$, which is consistent with that reported in Ref. 23.

B. The dependence of T_c on Nb concentration x

Figure 2 presents the temperature dependence of the electrical resistivity $\rho(T)$ [Fig. 2(a)], magnetic susceptibility $\chi(T)$ [Fig. 2(b)], and specific heat $C_p(T)$ [Fig. 2(c)] for Nb_xRe_{1-x} ($x = 0.18$, 0.25, 0.29, and 0.31). A pronounced superconducting transition is observed in all these quantities for each compound. Note that the superconducting transition is broadened upon increasing x, which is likely attributed to the enhanced sample inhomogeneity. Bulk SC with nearly 100% shielding volume can be inferred from the magnetic

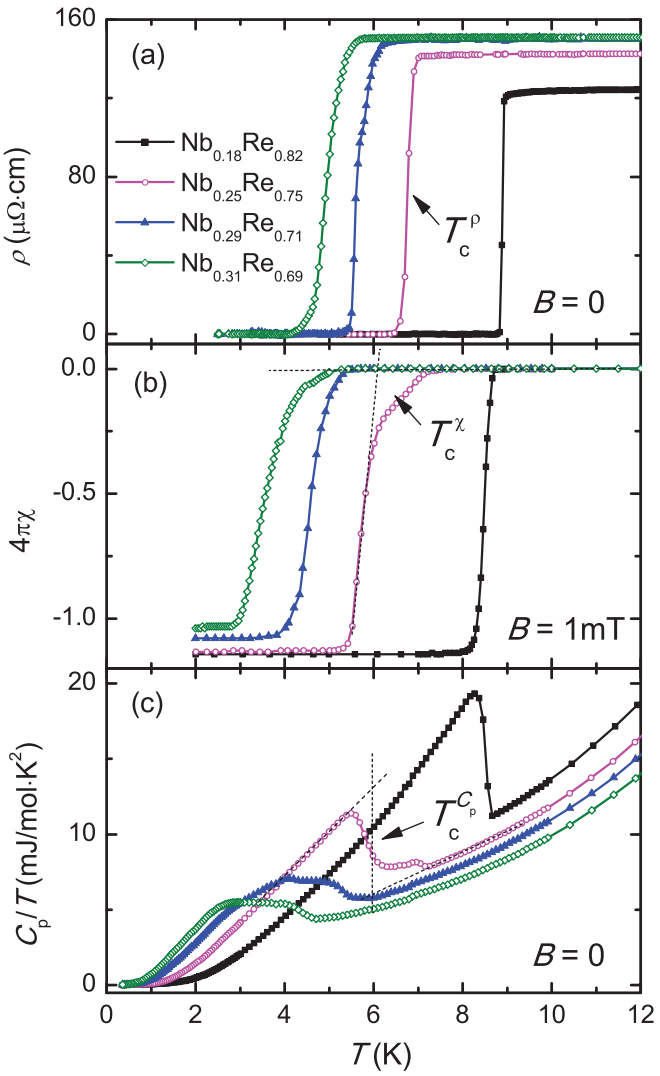

FIG. 2. (Color online) Temperature dependence of (a) the electrical resistivity $\rho(T)$, (b) the magnetic susceptibility $\chi(T)$, and (c) the specific heat $C_p(T)$ for Nb_xRe_{1-x} ($x = 0.18$, 0.25, 0.29, and 0.31). Dashed lines illustrate the methods of determining T_c.

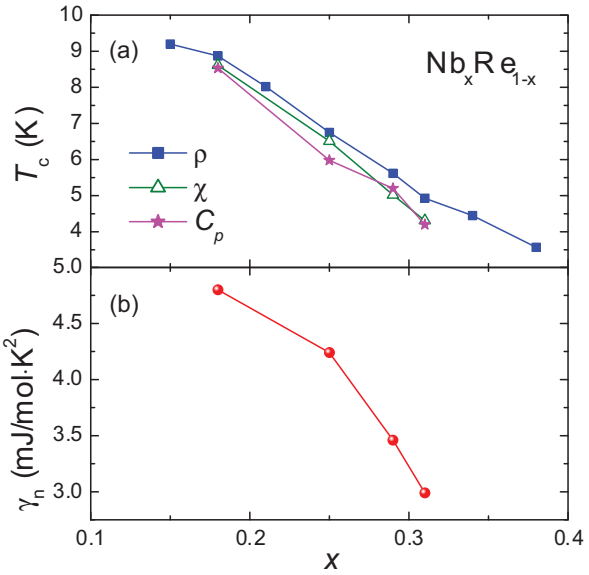

FIG. 3. (Color online) (a) T_c vs x for Nb_xRe_{1-x}, determined from the electrical resistivity $\rho(T)$, the magnetic susceptibility $\chi(T)$, and the specific heat $C_p(T)$, respectively. (b) The Sommerfeld coefficient $\gamma_n(x)$ plotted as a function of x.

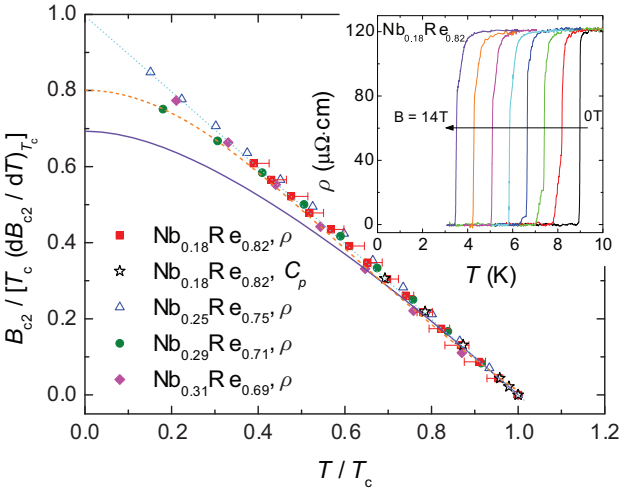

FIG. 4. (Color online) Normalized upper critical field $B_{c2}/[T_c(dB_{c2}/dT)_{T_c}]$ vs T/T_c for Nb_xRe_{1-x} ($x = 0.18$, 0.25, 0.29, and 0.31). The solid and dashed lines represent fits of the WHH and GL methods, respectively. The inset shows the electrical resistivity $\rho(T)$ of $Nb_{0.18}Re_{0.82}$ at various magnetic fields.

susceptibility as well as the specific-heat jumps at T_c. The Sommerfeld coefficient γ_n can be derived from the polynomial fits of the normal-state specific heat by $C_p = \gamma_n T + (B_3T^3 + B_5T^5 + B_7T^7)$, in which the first term represents the electronic contribution $C_e = \gamma_n T$, while the second term denotes the phonon contribution. With this method, we obtain $\gamma_n = 4.8$ mJ/mol K^2 for $x = 0.18$, the γ_n value decreasing with increasing x. It is pointed out that a much larger value of $\gamma_n = 53.5$ mJ/mol K^2 was previously reported in Ref. 23 for $Nb_{0.18}Re_{0.82}$, presumably due to a miscalculation. Furthermore, no evidence of magnetic order and magnetic impurities is observed in the above measurements.

In Fig. 3, we plot the superconducting transition temperatures T_c and the Sommerfeld coefficient γ_n as a function of the Nb content x for Nb_xRe_{1-x}. Here we determine T_c from the intersections of the magnetic susceptibility, and the midpoints of the resistive transition and the specific-heat jumps as illustrated in Fig. 2. One can see that the bulk T_c's, derived from the magnetic susceptibility and specific heat, are slightly reduced but still compatible with the resistive T_c, showing a monotonic decrease with increasing x. Such dependence of $T_c(x)$ may originate from the decrease of the density of states at the Fermi level, as reflected by the x dependence of $\gamma_n(x)$ in Fig. 3(b).

C. Upper critical field

To determine the upper critical field $B_{c2}(T)$, we have measured the electrical resistivity $\rho(T)$ ($x = 0.18$, 0.25, 0.29, and 0.31) and specific heat $C_p(T)$ ($x = 0.18$) at various magnetic fields. As an example, we show $\rho(T)$ of $Nb_{0.18}Re_{0.82}$ at magnetic fields up to 14 T in the inset of Fig. 4. Obviously, the superconducting transition is shifted to lower temperatures upon increasing magnetic field, but not yet suppressed by the maximum field of 14 T we applied. The superconducting transition of $x = 0.18$ remains fairly sharp in a magnetic field, but it is broadened in other samples with larger x, indicating that the samples become more inhomogeneous with increasing Nb content. Similar behavior is also seen in the specific-heat data (see below).

In the main panel of Fig. 4, we show the normalized upper critical field $B_{c2}/[T_c(dB_{c2}/dT)_{T_c}]$ versus T/T_c for various Nb contents. Here the resistive T_c and the horizontal bars are determined from the midpoints, as well as the 10% and 90% drops of the normal-state resistivity just above T_c. The values of T_c from the specific heat are determined by using the entropy balance method in a plot of C/T vs T. Remarkably, the upper critical fields $B_{c2}(T)$, derived either from the same measurement of different sample concentrations x or from different measurements of the same sample ($x = 0.18$), can be nicely scaled by T_c; the normalized curves collapse onto a single line as shown in Fig. 4.

Another important feature of the upper critical field curve $B_{c2}(T)$ is the remarkably linear temperature dependence down to the base temperature $T \simeq 0.3$ K. For comparison, in Fig. 4 we include the fits of the upper critical fields by the Werthamer-Helfand-Hohenberg (WHH) method in the dirty limit (solid line)[26] as well as the Ginzburg-Landau (GL) formula,[27] $B_{c2}(T) = B_{c2}(0)[1 - (T/T_c)^2]/[1 + (T/T_c)^2]$ (dashed line). One can see that the WHH method fails to describe the experimental data over a wide temperature region. The GL formula can give a much better illustration of the experimental data, but also shows deviations at low temperatures. We estimate the upper critical field $B_{c2}(0)$ by linearly extrapolating $B_{c2}(T)$ to zero temperature, which gives $B_{c2}(0) = 23$, 14.5, 11.8, and 9 T for $x = 0.18$, 0.25, 0.29, and 0.31, respectively. Such values of $B_{c2}(0)$ largely exceed the corresponding orbital limiting field, and are close to or even larger than the Pauli limiting field.

According to the WHH theory,[26] the upper critical field limited by the orbital mechanism can be estimated from T_c

and the initial slope of the upper critical field $B_{c2}(T)$, i.e.,

$$B_{c2}^{\rm orb}(0) = -0.69T_c(dB_{c2}/dT)_{T=T_c}. \quad (1)$$

The above formula gives $B_{c2}^{\rm orb}(0) = 16.1$, 10.5, 8.6, and 6.3 T for $x = 0.18$, 0.25, 0.29, and 0.31, respectively.

On the other hand, SC can be destroyed by the Pauli paramagnetic effect in a magnetic field as a result of the Zeeman effect. The Pauli limiting field is usually defined by[28,29]

$$B_{c2}^{P}(0) = \Delta_0/\sqrt{2}\mu_B, \quad (2)$$

where Δ_0 is the energy gap amplitude at zero temperature. For a conventional BCS superconductor, $\Delta_0 = 1.76T_c$, Eq. (2) can be simplified as $B_{c2}^{P}(0) = 1.86T_c$. In the following section, we will show that Nb_xRe_{1-x} is a type of weak-coupling BCS superconductor. The Pauli limiting fields are, therefore, estimated to be 16.6, 12.6, 10.4, and 9.1 T for $x = 0.18$, 0.25, 0.29, and 0.31, respectively.

The linear temperature dependence of $B_{c2}(T)$ and the absence of Pauli limiting behavior are unusual for a BCS-type superconductor. However, similar behavior was also observed in other weakly correlated NCS superconductors. For example, a very large upper critical field $B_{c2}(0)$ was also reported in the multigap superconductors La_2C_3 (Ref. 30) and Y_2C_3.[15] In the latter case, evidence of line nodes was observed in the low-temperature limit.[15] In the following, we will provide further experimental facts to reveal the gap symmetry in Nb_xRe_{1-x} by measuring the low-temperature specific heat at various magnetic fields $C_p(T,B)$ as well as the London penetration depth $\Delta\lambda(T)$. Since the sample $Nb_{0.18}Re_{0.82}$ shows the highest sample quality among this series of compounds, we will focus on this concentration here, although other samples demonstrate similar behavior.

D. Gap symmetry

1. *Specific heat*

The temperature dependence of the specific heat $C_p(T)$ was previously reported for $Nb_{0.18}Re_{0.82}$ at zero field by Karki *et al.*[23] It shows exponential behavior in the low-temperature limit, suggesting BCS-type SC with a moderate electron-phonon coupling. In our measurements, similar behavior is observed for Nb_xRe_{1-x} [see Figs. 2(c) and 5(a)]. Upon increasing the Nb content from $x = 0.18$ to 0.31, the specific-heat jump $\Delta C/\gamma_n T_c$ at T_c varies from 1.86 to about 0.5. Note that the broadened superconducting transitions for samples with large x do not allow us to reliably determine the specific-heat jumps accurately enough. Far below the superconducting transition ($T < 0.3T_c$), the electronic specific heat $C_e(T)/T$ for various Nb contents shows a very weak temperature dependence which can be reasonably fitted by the BCS-type exponential behavior. Following the procedures described in Ref. 19, in Fig. 5(a) we fit the specific heat $C_e(T)/T$ of $Nb_{0.18}Re_{0.82}$ from the base temperature up to T_c, in which $C_e(T)/T$ data can be nicely described by the one-gap BCS model with an energy gap of $\Delta_0 = 1.93T_c$.

We further characterize the superconducting pairing state of $Nb_{0.18}Re_{0.82}$ by measuring the specific heat in a magnetic field. A pronounced upturn in $C_p(T)/T$ appears at low temperatures, which shifts to higher temperatures upon increasing magnetic field. This is ascribed to the high-T tail of a nuclear Schottky anomaly. In this case, the total specific heat can be expressed as $C_p(T,B) = C_e(T,B) + C_{\rm ph}(T) + C_{\rm Sch}(T,B)$, where $C_e(T,B)$, $C_{\rm ph}(T)$, and $C_{\rm Sch}(T,B)$ represent the electron, phonon, and nuclear Schottky contributions, respectively. The phonon contributions can be subtracted from the polynomial fits above T_c as illustrated in Sec. III B. The nuclear Schottky contribution follows the expression of $C_{\rm Sch}(T,B) = aB^2/T^2$, which can be subtracted by fitting the low-temperature specific-heat data [see Fig. 5(a), data for $B = 7$ T]. In Fig. 5(b), we plot the temperature dependence of the electronic specific heat $C_e(T)$ at various magnetic fields for $Nb_{0.18}Re_{0.82}$, as obtained after subtraction of the phonon and nuclear contributions. One can see that application of a magnetic field eventually shifts the sharp superconducting transition to lower temperatures and enhances the residual Sommerfeld coefficient $\gamma_0(B)$. Note that the specific-heat data at zero field show an extremely small residual Sommerfeld coefficient of $\gamma_0 = 0.018$ mJ/mol K^2, confirming the good quality of the sample. The inset of Fig. 5(b) presents the field dependence of the residual Sommerfeld coefficient $\gamma_0(B)$, which shows a remarkably linear field dependence, providing strong evidence of BCS-type SC for $Nb_{0.18}Re_{0.82}$. In fully gapped superconductors, the low-lying excitations are usually confined to the vortex cores, and the specific heat is proportional to the vortex density which increases linearly with increasing magnetic field, i.e., $\gamma_0(B) \sim B$.[31]

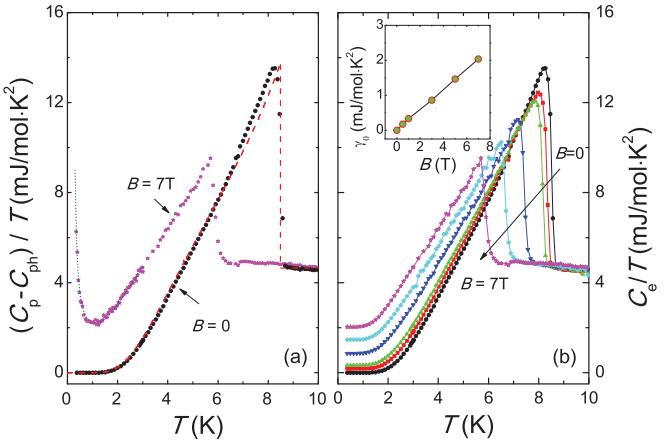

FIG. 5. (Color online) Temperature dependence of the specific heat at various magnetic fields for $Nb_{0.18}Re_{0.82}$. (a) The specific heat C_p obtained after subtracting the phonon contribution from the raw data at $B = 0$ and 7 T. The dashed line shows a fit to the BCS model with $\Delta_0 = 1.93T_c$. The dotted line denotes a power-law fit of the nuclear Schottky contributions $C_{\rm Sch}(T,B)$ at low temperatures. (b) The electronic specific heat $C_e(T)$ at $B = 0$, 0.5, 1, 3, 5, and 7 T. The inset plots the magnetic field dependence of the residual Sommerfeld coefficient $\gamma_0(B)$.

2. *London penetration depth*

While the specific heat $C_p(T)/T$ explores the quasiparticle density of states, the London penetration depth probes the superfluid density $\rho_s(T)$. In this section, we present a precise measurement of the penetration depth changes $\Delta\lambda(T)$ as well as $\rho_s(T)$ for $Nb_{0.18}Re_{0.82}$ by using a TDO-based technique.

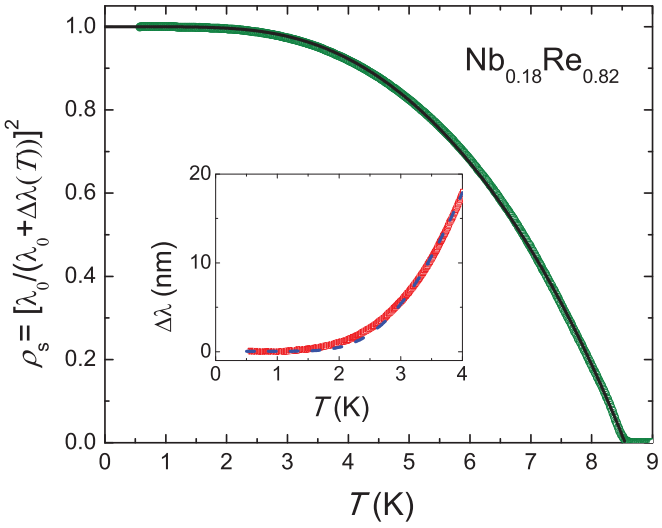

FIG. 6. (Color online) Temperature dependence of the superfluid density $\rho_s(T)$ for $Nb_{0.18}Re_{0.82}$. The inset shows the penetration depth $\Delta\lambda(T)$ at low temperatures. The lines represent fits to the BCS model.

With this method, the change of the London penetration depth $\Delta\lambda(T)$ is proportional to the resonant frequency shift $\Delta f(T)$, i.e., $\Delta\lambda(T) = G\,\Delta f(T)$, where the G factor is a constant, solely determined by the sample and coil geometries.[25] The inset of Fig. 6 shows the penetration depth $\Delta\lambda(T)$ at low temperatures for $Nb_{0.18}Re_{0.82}$, where $G = 1.4$ nm/Hz. A sharp superconducting transition with $T_c^{\rm TDO} = 8.7$ K is observed in this sample (not shown), which is highly consistent with all the other measurements. The penetration depth exhibits very weak temperature dependence at low temperatures. According to the isotropic BCS model, the penetration depth $\Delta\lambda(T)$ can be approximated by the following exponential temperature dependence at $T \ll T_c$: $\Delta\lambda(T) = \lambda(T) - \lambda_0 = \lambda_0\sqrt{\frac{\pi\Delta_0}{2T}}e^{-\frac{\Delta_0}{T}}$, where λ_0 and Δ_0 are the penetration depth and gap amplitude at zero temperature, respectively. In the inset of Fig. 6, the dashed line shows a fit of the BCS model to our experimental data $\Delta\lambda(T)$. Here we fix $\lambda_0 = 414$ nm as estimated below, and the derived energy gap of $\Delta_0 = 1.91T_c$ is remarkably consistent with that from the specific-heat data.

To further analyze the superconducting gap symmetry, in the following we turn to the superfluid density $\rho_s(T)$ of $Nb_{0.18}Re_{0.82}$. The normalized superfluid density can be converted from the penetration depth by $\rho_s(T) = [\lambda_0/\lambda(T)]^2$. Here we estimate the value of λ_0 according to the BCS and Ginzburg-Landau theories for a type-II superconductor,[32] i.e., $\lambda_0 = \frac{1}{1.76T_c}\sqrt{\frac{\Phi_0 B_{c2}(0)}{24\gamma_n}}$, where Φ_0 is the magnetic flux quantum. By taking the parameters derived from our specific-heat data, i.e., $T_c^{C_p} = 8.5$ K, $B_{c2}^{C_p}(0) = 22.85$ T, and $\gamma_n = 4.8$ mJ/mol $K^2 = 0.51 \times 10^4$ erg/cm^3 K^2, we derived $\lambda_0 = 414$ nm for $Nb_{0.18}Re_{0.82}$, which is compatible with that obtained from the measurements of the lower critical field.[23] In the main panel of Fig. 6, we plot the temperature dependence of the superfluid density $\rho_s(T)$ for $Nb_{0.18}Re_{0.82}$.

In order to adopt a proper model to fit the superfluid density $\rho_s(T)$, we estimated the mean free path ($l \approx 5$ nm) and the coherence length ($\xi_0 \approx 4$ nm) of the $Nb_{0.18}Re_{0.82}$ sample from the resistivity $\rho(T_c) = 120\ \mu\Omega$ cm, and the above mentioned quantities of $T_c^{C_p}$, $B_{c2}^{C_p}(0)$, and γ_n.[33] The close values of the mean free path and the coherence length suggest that it is appropriate to treat the sample in the dirty limit. Accordingly, we analyze our superfluid density $\rho_s(T)$ in terms of the s-wave weak-coupling BCS model in the dirty limit,[27] i.e.,

$$\rho_s(T) = \frac{\Delta(T)}{\Delta_0}\tanh\left(\frac{\Delta(T)}{2T}\right). \quad (3)$$

Here the temperature dependence of the gap function is given by[34]

$$\Delta(T) = \Delta_0\tanh\left[\frac{\pi T_c}{\Delta_0}\sqrt{a\frac{\Delta C}{C_e}\left(\frac{T_c}{T}-1\right)}\right], \quad (4)$$

where $\Delta C/C_e$ is the relative jump in the electronic specific heat at T_c and $a = 2/3$ for an isotropic BCS superconductor. As shown in Fig. 6, the experimental data $\rho_s(T)$ of $Nb_{0.18}Re_{0.82}$ can be well described by the BCS model with a gap magnitude of $\Delta_0 = 1.95T_c$, which agrees well with the values derived from our fits of the specific-heat and penetration depth data, as well as the previous NMR data.[24] These measurements clearly identify $Nb_{0.18}Re_{0.82}$ as an s-wave BCS superconductor. We note that similar results were also obtained for $Nb_{0.29}Re_{0.71}$, suggesting BCS-like SC for Nb_xRe_{1-x} ($0.13 \leqslant x \leqslant 0.38$).

IV. CONCLUSION

In summary, we have studied the superconducting properties of the NCS compounds Nb_xRe_{1-x} ($0.13 \leqslant x \leqslant 0.38$) by measuring the electrical resistivity, magnetic susceptibility, specific heat, as well as the London penetration depth. We found that the superconducting transition temperature T_c decreases monotonically with increasing x, which is partially attributed to the decrease of the density of states at the Fermi energy. The upper critical field $B_{c2}(T)$ of Nb_xRe_{1-x} can be perfectly scaled by the corresponding T_c, showing a rather linear temperature dependence down to the base temperature. The upper critical field at zero temperature $B_{c2}(0)$ exceeds the orbital limit, and also approaches the Pauli paramagnetic limit. On the other hand, the temperature dependence of the electronic specific-heat coefficient $C_e(T)/T$, penetration depth $\Delta\lambda(T)$, and superfluid density $\rho_s(T)$ of $Nb_{0.18}Re_{0.82}$ can be consistently described by the BCS model with an energy gap of $\Delta_0 \approx 1.9T_c$. Evidence of BCS SC for $x = 0.18$ is further provided by the observation of a linear field dependence of the residual Sommerfeld coefficient $\gamma_0(B)$. Our results demonstrate that Nb_xRe_{1-x} ($0.13 \leqslant x \leqslant 0.38$) is an s-wave BCS-type superconductor with negligible contributions from the spin-triplet component, in spite of the heavy atomic mass of Re residing on the NCS sites. The observation of s-wave superconductivity with an extremely large $B_{c2}(0)$ in Nb_xRe_{1-x}, which is rare among the NCS superconductors, demands further theoretical and experimental investigations.

ACKNOWLEDGMENTS

We appreciate valuable discussions with L. Z. Sun and M. B. Salamon. This work was supported by the National Basic Research Program of China (Grants No. 2011CBA00103 and

No. 2009CB929104), the Natural Science Foundation of China (Grant No. 10934005), Zhejiang Provincial Natural Science Foundation of China, the Fundamental Research Funds for the Central Universities, and the Max Planck Society under the auspices of the Max Planck Partner Group of the MPI for Chemical Physics of Solids, Dresden.

*hqyuan@zju.edu.cn

[1] E. Bauer, G. Hilscher, H. Michor, Ch. Paul, E. W. Scheidt, A. Gribanov, Yu. Seropegin, H. Noël, M. Sigrist, and P. Rogl, Phys. Rev. Lett. **92**, 027003 (2004).
[2] L. P. Gor'kov and E. I. Rashba, Phys. Rev. Lett. **87**, 037004 (2001).
[3] S. K. Yip, Phys. Rev. B **65**, 144508 (2002).
[4] P. A. Frigeri, D. F. Agterberg, A. Koga, and M. Sigrist, Phys. Rev. Lett. **92**, 097001 (2004).
[5] Y. Yanase and M. Sigrist, J. Phys. Soc. Jpn. **76**, 124709 (2007).
[6] S. Fujimoto, J. Phys. Soc. Jpn. **76**, 051008 (2007).
[7] H. Q. Yuan, D. F. Agterberg, N. Hayashi, P. Badica, D. Vandervelde, K. Togano, M. Sigrist, and M. B. Salamon, Phys. Rev. Lett. **97**, 017006 (2006); H. Q. Yuan, M. B. Salamon, P. Badica, and K. Togano, Physica B **403**, 1138 (2008).
[8] M. Nishiyama, Y. Inada, and G. Q. Zheng, Phys. Rev. Lett. **98**, 047002 (2007).
[9] H. Takeya, M. El Massalami, S. Kasahara, and K. Hirata, Phys. Rev. B **76**, 104506 (2007).
[10] X. L. Qi, T. L. Hughes, S. Raghu, and S. C. Zhang, Phys. Rev. Lett. **102**, 187001 (2009).
[11] C. K. Lu and S. Yip, Phys. Rev. B **82**, 104501 (2010).
[12] E. Bauer and M. Sigrist, *Non-centrosymmetric Superconductors: Introduction and Overview* (Springer, Berlin, 2012).
[13] M. Sigrist, D. F. Agterberg, P. A. Frigeri, A. Hayashi, R. P. Kaur, A. Koga, I. Milat, K. Wakabayashi, and Y. Yanase, J. Magn. Magn. Mater. **310**, 536 (2007).
[14] H. Mukuda, T. Ohara, M. Yashima, Y. Kitaoka, R. Settai, Y. Ōnuki, K. M. Itoh, and E. E. Haller, Phys. Rev. Lett. **104**, 017002 (2010).
[15] J. Chen, M. B. Salamon, S. Akutagawa, J. Akimitsu, J. Singleton, J. L. Zhang, L. Jiao, and H. Q. Yuan, Phys. Rev. B **83**, 144529 (2011).
[16] A. Harada, S. Akutagawa, Y. Miyamichi, H. Mukuda, Y. Kitaoka, and J. Akimitsu, J. Phys. Soc. Jpn. **76**, 023704 (2007).
[17] S. Kuroiwa, Y. Saura, J. Akimitsu, M. Hiraishi, M. Miyazaki, K. H. Satoh, S. Takeshita, and R. Kadono, Phys. Rev. Lett. **100**, 097002 (2008).
[18] T. Klimczuk, F. Ronning, V. Sidorov, R. J. Cava, and J. D. Thompson, Phys. Rev. Lett. **99**, 257004 (2007).
[19] J. Chen, L. Jiao, J. L. Zhang, Y. Chen, L. Yang, M. Nicklas, F. Steglich, and H. Q. Yuan, New J. Phys. **15**, 053005 (2013).
[20] N. Kimura, K. Ito, H. Aoki, S. Uji, and T. Terashima, Phys. Rev. Lett. **98**, 197001 (2007).
[21] R. Settai, Y. Miyauchi, T. Takeuchi, F. Lvy, T. Sheikin, and Y. Ōnuki, J. Phys. Soc. Jpn. **77**, 073705 (2008).
[22] A. G. Knapton, J. Less-Common Met. **1**, 480 (1959).
[23] A. B. Karki, Y. M. Xiong, N. Haldolaarachchige, S. Stadler, I. Vekhter, P. W. Adams, D. P. Young, W. A. Phelan, and J. Y. Chan, Phys. Rev. B **83**, 144525 (2011).
[24] C. S. Lue, T. H. Su, H. F. Liu, and B. L. Young, Phys. Rev. B **84**, 052509 (2011).
[25] R. Prozorov, R. W. Giannetta, P. Fournier, and R. L. Greene, Phys. Rev. Lett. **85**, 3700 (2000), and references therein.
[26] N. R. Werthamer, E. Helfand, and P. C. Hohenberg, Phys. Rev. **147**, 295 (1966).
[27] M. Tinkham, *Introduction to Superconductivity*, 2nd ed. (McGraw-Hill, New York, 1996).
[28] A. M. Clogston, Phys. Lett. **9**, 266 (1962).
[29] B. S. Chandrasekhar, J. Appl. Phys. Lett. **1**, 7 (1962).
[30] J. S. Kim, R. K. Kremer, O. Jepsen, and A. Simon, Curr. Appl. Phys. **6**, 897 (2006).
[31] C. Caroli, P. G. de Gennes, and J. Matricon, Phys. Lett. **9**, 307 (1964).
[32] F. Gross, B. S. Chandrasekhar, D. Einzel, K. Andres, P. J. Hirschfeld, H. R. Ott, J. Beuers, Z. Fisk, and J. L. Smith, Z. Phys. B: Condens. Matter **64**, 175 (1986).
[33] T. P. Orlando, E. J. McNiff, Jr., S. Foner, and M. R. Beasley, Phys. Rev. B **19**, 4545 (1979).
[34] R. Prozorov and R. W. Giannetta, Supercond. Sci. Technol. **19**, R41 (2006).